JOURNAL OF GEOPHYSICAL RESEARCH: ATMOSPHERES, VOL. 118, 6444–6453, doi:10.1002/jgrd.50504, 2013

Use of spaceborne lidar for the evaluation of thin cirrus contamination and screening in the Aqua MODIS Collection 5 aerosol products

Jingfeng Huang,[1,2] N. Christina Hsu,[3] Si-Chee Tsay,[3] Zhaoyan Liu,[4,5] Myeong-Jae Jeong,[6] Richard A. Hansell,[1,3] and Jaehwa Lee [1,3]

Received 3 October 2012; revised 13 May 2013; accepted 16 May 2013; published 20 June 2013.

[1] Cloud contamination from subvisual thin cirrus clouds is still a challenging issue for operational satellite aerosol retrievals. In the A-Train constellation, concurrent high-sensitivity cirrus observations from the Cloud-Aerosol Lidar and Infrared Pathfinder Satellite Observations (CALIPSO) provide us with an unprecedented opportunity to examine the susceptibility of the Aqua Moderate Resolution Imaging Spectroradiometer (MODIS) aerosol retrievals to thin cirrus contamination and to evaluate the robustness of various cirrus screening techniques. Quantitative evaluations indicate that the current cirrus screening schemes in the MODIS Dark Target and Deep Blue Collection 5 aerosol retrievals can effectively remove most cirrus signals while some residual thin cirrus signals still exist with strong spatial and seasonal variability. Results also show significant linkage between thin cirrus occurrence frequency and the susceptibility of aerosol retrievals to thin cirrus contamination. Using the CALIPSO cirrus observations as a reference, we also examined the effectiveness and robustness of eight MODIS-derived cirrus screening parameters. These parameters include apparent reflectance at 1.38 μm (R1.38), cirrus reflectance at 0.66 μm (CR0.66), CR0.66 cirrus flag (CF), reflectance ratio between 1.38 μm and 0.66 μm (RR1.38/0.66), reflectance ratio between 1.38 μm and 1.24 μm (RR1.38/1.24), brightness temperature difference between 8.6 μm and 11 μm (BTD8.6–11), brightness temperature difference between 11 μm and 12 μm (BTD11–12), and cloud phase infrared approach (CPIR). Among these parameters, RR1.38/0.66 achieves the best overall performance, followed by the BTD11–12. Results from several test cases suggest that the cirrus screening schemes in the operational MODIS aerosol retrieval algorithms can be further improved to reduce thin cirrus contamination.

Citation: Huang, J., N. C. Hsu, S.-C. Tsay, Z. Liu, M.-J. Jeong, R. A. Hansell, and J. Lee (2013), Use of spaceborne lidar for the evaluation of thin cirrus contamination and screening in the Aqua MODIS Collection 5 aerosol products, *J. Geophys. Res. Atmos.*, *118*, 6444–6453, doi:10.1002/jgrd.50504.

1. Introduction

[2] Satellite data play irreplaceable roles in large-scale aerosol observations and relevant global climate change studies [e.g., *Andreae*, 1991; *Breon et al*., 2002; *Menon et al*., 2002]. However, uncertainties associated with satellite data retrieval algorithms are still not well quantified [e.g., *Myhre et al*., 2005]. For example, the existence of high thin cirrus clouds with small optical thickness is still sometimes misidentified as aerosols in the Moderate Resolution Imaging Spectroradiometer (MODIS) operational aerosol products [e.g., *Gao et al*., 2002a; Kaufman et al., 2005; *Huang et al*., 2011, 2012]. Satellite aerosol retrieval uncertainties [e.g., *Myhre et al*., 2005; *Jeong et al*., 2005; *Jeong and Li*, 2005] are also partially a cause for the inconsistency between model simulations and observational evidence of large-scale aerosol effects [*Takemura et al*., 2005; *Tao et al*., 2007]. Therefore, it is imperative to perform rigorous and systematic global evaluations of cirrus contamination in satellite aerosol products and to explore alternative schemes for cirrus screening.

[3] With concurrent cirrus observations from ground or spaceborne lidars, quantitative evaluation of thin cirrus contamination in the operational aerosol products becomes

[1]Earth System Science Interdisciplinary Center, UMD, College Park, Maryland, USA.
[2]Center for Satellite Applications and Research, NESDIS, NOAA, College Park, Maryland, USA.
[3]NASA Goddard Space Flight Center, Greenbelt, Maryland, USA.
[4]NASA Langley Research Center, Hampton, Virginia, USA.
[5]Science Systems and Applications Inc., Hampton, Virginia, USA.
[6]Department of Atmospheric and Environmental Sciences, Gangneung-Wonju National University, Gangneung, South Korea.

Corresponding author: J. Huang, Center for Satellite Applications and Research, NESDIS, NOAA, 5825, University Research Court, College Park, MD 20740, USA. (jingfeng.huang@noaa.gov)

2169-897X/13/10.1002/jgrd.50504

possible [e.g., *Huang et al*., 2011; *Huang et al*., 2012; *Chew et al*., 2011]. The advent of the A-Train satellite constellation [e.g., *L'Ecuyer and Jiang*, 2010] provides an unprecedented chance to comprehensively observe global cirrus cloud coverage and its temporal and spatial variability [e.g., *Sassen and Campbell*, 2001; *Sassen et al.*, 2008; *Massie et al*., 2010; *Jiang et al*., 2010]. Moreover, the Cloud-Aerosol Lidar and Infrared Pathfinder Satellite Observations (CALIPSO) is particularly suited for detecting high thin cirrus, because it is spaceborne and has fewer attenuation issues than ground-based lidar systems. The concurrent measurements from the Aqua Moderate Resolution Imaging Spectroradiometer (MODIS) and the CALIPSO enable examination of the susceptibility of the MODIS aerosol products to cirrus contamination and to evaluate the robustness of various MODIS-derived cirrus screening techniques. Compared to the ground-based lidar and sunphotometer, the significant increase of collocated observations from both active and passive sensors in the A-Train constellation allows for comprehensive investigative studies of these thin cirrus effects. Such evaluation and examination are valuable for algorithm improvements in terms of cirrus screening and cirrus contamination correction in the operational aerosol retrieval algorithms.

[4] Cirrus screening in the current operational MODIS Dark Target and Deep Blue Collection 5 aerosol algorithms primarily utilizes apparent reflectance at 1.38 μm which is very sensitive to high clouds due to the strong water vapor absorption at this wavelength [MOD04 ATBD; *Remer et al*., 2009; *Hsu et al*., 2006]. However, residual cirrus contamination in the operational aerosol products are still observed [e.g., *Gao et al*., 2002a; *Kaufman et al*., 2005; *Schaap et al*., 2009], which warrants the in-depth investigation in this study. A systematic evaluation of various MODIS-retrieved cirrus screening parameters and their corresponding threshold values is therefore desired.

[5] Cirrus clouds usually occur at higher altitudes (>10 km in the tropical region) and are commonly composed of ice crystals. Cirrus cloud identification based on apparent reflectance at 1.38 μm, 0.66 μm, 1.24 μm, and brightness temperature differences (BTD) between three thermal infrared channels (8.6, 11, and 12 μm) have been discussed in previous studies [e.g., *Gao and Kaufman*, 1995; *Gao et al*. 2002a, 2002b; *Roskovensky and Liou*, 2003; *Roskovensky et al*., 2004]. Apparent reflectance at 1.38 μm for cirrus detection is used because of strong water vapor absorption at this wavelength, which results in cirrus sensitive contrast between highly reflective cirrus at higher altitudes and a much smaller reflectance in noncirrus scenes owing to strong water vapor absorption at relatively lower altitudes. Because the sensitivity of water vapor absorption varies among different bands, reflectance from a second less absorbing channel is usually required for scaling the absorbing effects of water vapor in practical algorithms when apparent reflectance at 1.38 μm is used for detecting cirrus [*Gao et al*., 2002b].

[6] Our previous works focused on regional studies of thin cirrus contamination on aerosol optical depth retrievals during the Biomass-burning Aerosols in South East-Asia: Smoke Impact Assessment (BASE-ASIA) campaign [*Huang et al*., 2011] and also on evaluation studies of ground-based aerosol retrievals [*Huang et al*., 2012]. Extending our earlier work, this study aims to: (1) investigate the susceptibility of satellite aerosol measurements to cirrus contamination and to quantify its influence on a global scale by exploring the susceptibility of valid and quality assured aerosol retrievals to thin cirrus identification by pairing up MODIS and CALIPSO data; (2) evaluate and compare the effectiveness and robustness of several satellite retrieved cirrus screening parameters when they are used for global aerosol retrievals; (3) discuss selection of appropriate satellite-derived cirrus screening parameters for their use in operational algorithms and propose the preferred method. Section 2 introduces the main data sets used for this study, followed by section 3 that presents the results. Last, section 4 summarizes our main findings and conclusions.

2. Data and Data Processing

[7] The main data sets used for this study are satellite aerosol retrievals from Aqua MODIS and concurrent satellite cirrus observations from CALIPSO during July 2006–August 2011, a 62-month period. Additional MODIS L1B, water vapor, and cloud products are also employed for testing multiple cirrus screening parameters, for a 1 year period from December 2006 to November 2007.

2.1. MODIS

[8] For this study, Aqua MODIS data were utilized because Aqua flies in formation with CALIPSO in the A-Train constellation. The MYD021KM Level 1B Collection 5 data and MYD06 Level 2 Collection 5.1 data are used to test eight MODIS derived parameters that are potentially useful for cirrus screening. We also selected the Aqua MYD04 Level 2 Collection 5.1 data for aerosol retrievals and used the best quality ensured (quality flag = 3) AOT data at 550 nm (*Remer et al*., [2005, 2009] and *Levy et al*. [2010] for Dark Target AOT and *Hsu et al*., [2004, 2006] for Deep Blue AOT). The eight MODIS-derived cirrus screening parameters are apparent reflectance at 1.38 μm (R1.38), its derivative cirrus reflectance at 0.66 μm (CR0.66), cirrus flag (CF), reflectance ratio between 1.38 μm and 0.66 μm (RR1.38/0.66), reflectance ratio between 1.38 μm and 1.24 μm (RR1.38/1.24), brightness temperature difference between 8.6 μm and 11 μm (BTD8.6–11), brightness temperature difference between 11 μm and 12 μm (BTD11–12), and cloud phase infrared approach (CPIR). The cirrus flag, cloud phase infrared (CPIR) flag, and brightness temperature difference data are in the MYD06 cloud products [*Menzel et al.*, 2013], while Band 1 (0.66 μm), Band 5 (1.24 μm), and Band 26 (1.38 μm) data are in the MYD021KM Level 1B products.

2.2. CALIPSO

[9] CALIPSO combines an active lidar instrument (CALIOP) with passive infrared and visible imagers to probe the vertical structure and properties of clouds and aerosols over the globe [*Vaughan et al*., 2005, 2009; *Young and Vaughan*, 2009; *Winker et al*., 2010; *Yorks et al*., 2011]. CALIPSO lags Aqua by 1–2 min in the A-Train constellation [*L'Ecuyer and Jiang*, 2010]. Compared to the 10 km along-track spatial resolution of the MODIS C5.1 aerosol products at nadir, the CALIOP ground footprint is 70 m in diameter. The CALIPSO vertical feature mask (VFM) product has a

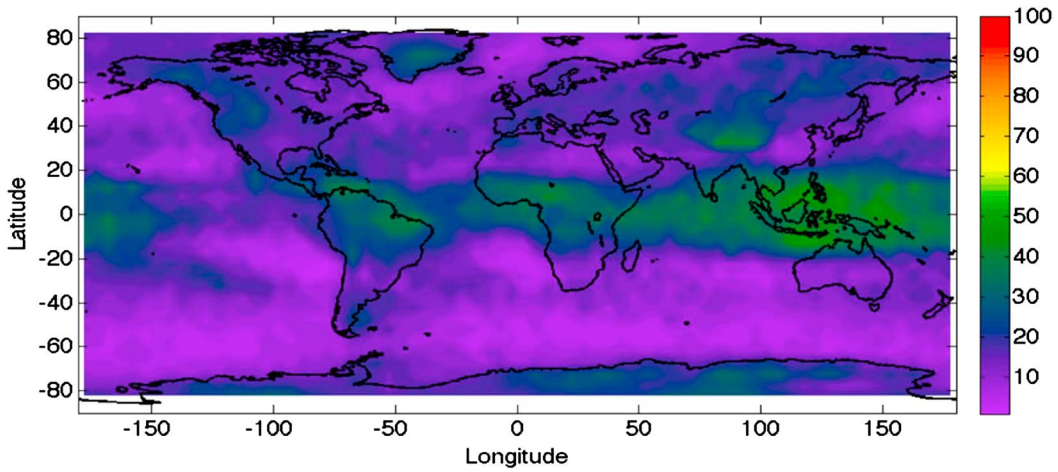

Figure 1. Daytime thin cirrus occurrence frequency (%) as calculated from CALIPSO VFM.

horizontal spacing of 333 m, but the horizontal resolution varies with altitude (h): 333 m up to h = 8.2 km, 1 km from h = 8.2 km to 20.2 km, and 1.667 km from h = 20.2 km to 30.1 km. Its vertical resolution also varies with altitude: 30 m up to h = 8.2 km, 60 m from h = 8.2 km to 20.2 km, and 180 m from h = 20.2 km to 30.1 km [*Liu et al*., 2005; 2009]. This provides a unique opportunity to closely examine the vertical profiles of both aerosol and clouds. For this study, the version 3.01 CALIPSO Level 2.0 VFM data, which include a "transparent thin cirrus" cloud subtype [*Liu et al*., 2005, 2009], are used as a baseline for cirrus cloud detection. Although CALIPSO provides both daytime and nighttime measurements, only daytime CALIPSO data spanning July 2006–August 2011 are used in this study, because the Aqua MODIS aerosol products are only available during daytime.

3. Results

3.1. MODIS Versus CALIPSO

[10] Daytime thin cirrus occurrence frequency was first inferred from the CALIPSO VFM based on the following three criteria [*Huang et al*., 2011]:

[11] 1. the confidence levels for a feature reported in VFM have to be high with the cloud-aerosol discrimination score greater than 70 to ensure high detection confidence;

[12] 2. the feature type is "cloud", and the feature subtype is "transparent cirrus clouds"; and

[13] 3. the surface return signal is detected ensuring that the detected cirrus cloud is optically thin [*Sassen et al*., 2008].

[14] Figure 1 shows prevalent thin cirrus over the global tropics, particularly over the tropical Indian Ocean, Maritime Continents, tropical Western Pacific, Central Africa, and

Table 1. Global Averages of the Susceptibility of Aqua MODIS MYD04 Collection 5 Level 2 AOT Retrievals to Thin Cirrus Contamination, and Its Seasonality and Sensitivity to Cloud Fraction, for the Period of July 2006–August 2011[a]

	DJF		MAM		JJA		SON		All Seasons	
	SW	GW	SW	GW	SW	GW	SW	GW	SW	GW
DT_SP	3.03%	4.06%	3.68%	5.23%	3.11%	4.62%	2.97%	4.11%	**3.19%**	**4.50%**
DT_SP_L	16.21%	15.52%	15.81%	17.74%	9.89%	12.93%	12.37%	13.56%	**12.70%**	**13.99%**
DT_SP_O	1.97%	2.05%	2.29%	2.25%	1.61%	1.96%	1.86%	1.76%	**1.93%**	**1.94%**
DB_SP	6.78%	7.99%	6.83%	11.69%	4.25%	9.84%	5.54%	9.49%	**5.73%**	**10.94%**
DT_dAOT	0.0506	0.0834	0.0647	0.0899	0.0729	0.0649	0.0490	0.0817	**0.0603**	**0.0876**
DT_dAOT_L	0.0405	0.0668	0.0781	0.0967	0.0864	0.0705	0.0581	0.0570	**0.0715**	**0.0712**
DT_dAOT_O	0.0423	0.0852	0.0524	0.0924	0.0523	0.0610	0.0372	0.0856	**0.0467**	**0.0906**
DB_dAOT	0.0540	0.0846	0.1032	0.0719	0.0729	0.0874	0.0575	0.0907	**0.0719**	**0.0931**
DT_dAE_O	−0.2308	−0.2200	−0.1024	−0.1852	−0.1745	−0.2182	−0.2453	−0.2199	**−0.1912**	**−0.2431**
DT_dFMF_O	−0.0777	−0.0700	−0.0223	−0.0512	−0.0478	−0.0588	−0.0748	−0.0706	**−0.0573**	**−0.0699**
DB_dAE	−0.1256	−0.1080	−0.1922	−0.0991	−0.0904	−0.0581	−0.1167	−0.0567	**−0.1356**	**−0.0450**

[a]SP, Susceptibility %; L, Land; O, Ocean; DT, Dark Target; DB, Deep Blue; SW, Sample-Weighted; GW, Grid Weighted; dAOT (or dAE, or dFMF), AOT (or AE, or FMF) Difference Between Cirrus-Contaminated and Cirrus-Free Cases; CF, Cloud Fraction. "Sample-weighted" means the statistics were calculated based on the samples, and samples could be different from grid to grid, and from land to ocean; "Grid-weighted" means the statistics were calculated after the samples are gridded at each 5° × 5° grid, thus the statistical contribution from each grid is equal. The SP values were evaluated from the conservative approach that assumes thin cirrus contamination can be successfully self-contained through aggregations in the aerosol retrievals with subpixel cloud fraction >0. The difference between "cirrus-contaminated cases" and "cirrus-free cases" were calculated based on CF = 0 retrievals only. Please note that the cloud fraction information used in the statistics is from Dark Target algorithm although it covers both Dark Target and Deep Blue aerosol retrieval regions. The results from the "All Seasons" data analysis are highlighted in bold.

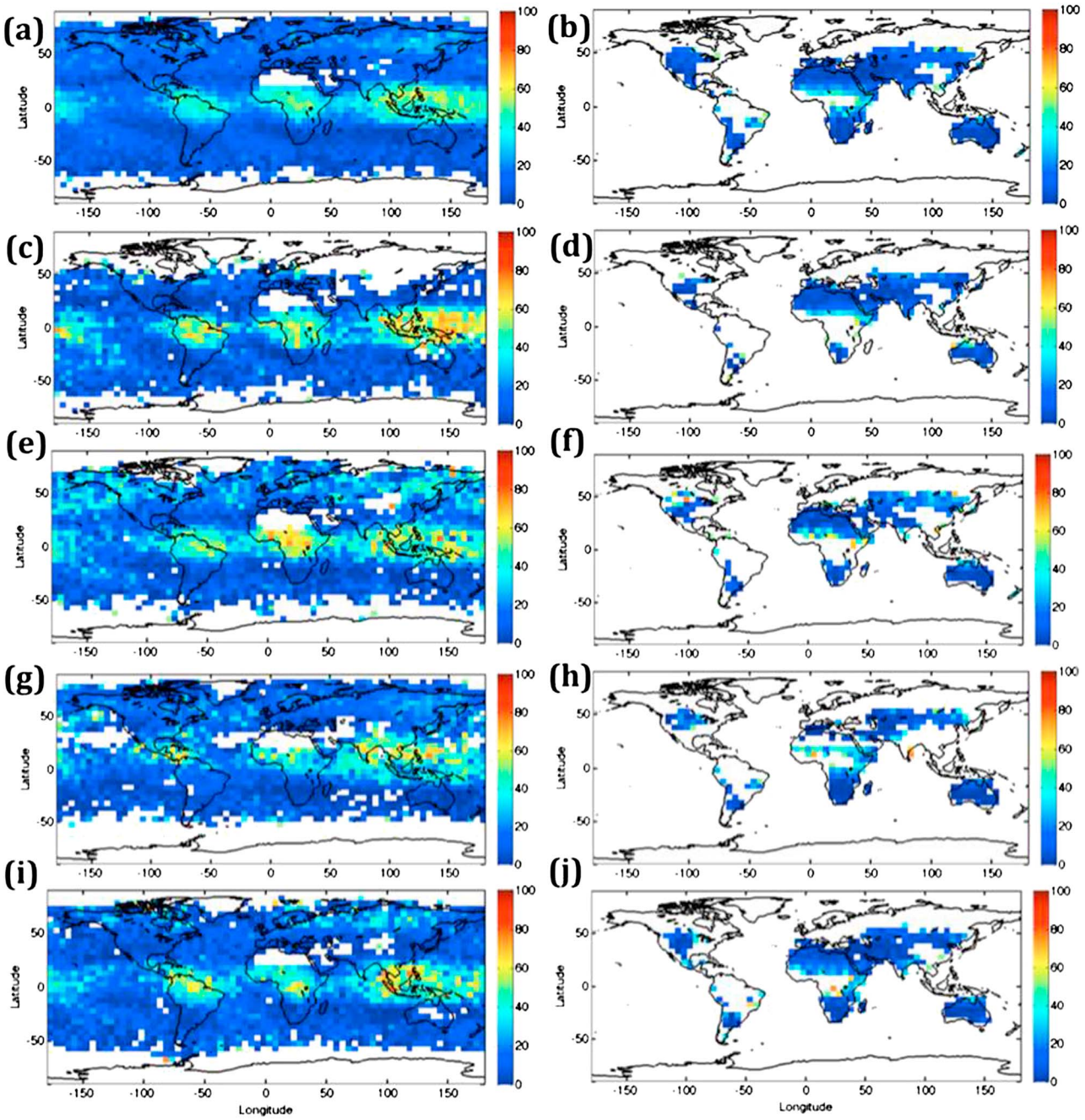

Figure 2. Susceptibility percentage (SP, %) of Aqua MODIS (left) Dark Target and (right) Deep Blue AOT retrievals testing against CALIPSO vertical feature mask. (a, b) All seasons, (c, d) DJF, (e, f) MAM, (g, h) JJA, and (i, j) SON.

Northern South America. There were also thin cirrus occurrences observed by CALIPSO over Greenland, the Himalayas, and Antarctic, where there are very rare MODIS aerosol retrievals due to snow and ice screening, high solar zenith angle screening, or high terrain surface complexity. Therefore, it is expected that higher susceptibility of aerosol retrievals to thin cirrus would occur over the global tropics.

[15] Collocating MODIS and CALIPSO data is performed on a per-pixel basis employing a two-step approach. First, on the temporal scale, locate all of the corresponding MODIS granules that overlap a particular CALIPSO track. Because both Aqua and CALIPSO are in the A-Train constellation and they are only 1–2 min apart, this first step of temporal collocation assures the temporal proximity of the two sensor observations. Second, on the spatial scale, match up the best quality MODIS C5 aerosol product pixels that contain the CALIPSO footprint. In this step, distances from the concurrent MODIS observation to each CALIPSO footprint are calculated and sorted, and the closest MODIS/CALIPSO coincidence in distance is selected. Only quality filtered MODIS aerosol retrievals (QA = 3 over land and QA = 1–3 over ocean) in cloud-free (cloud fraction is zero) pixels are used. This process is repeated for every CALIPSO track in the 62-month period, from July 2006 to August 2011.

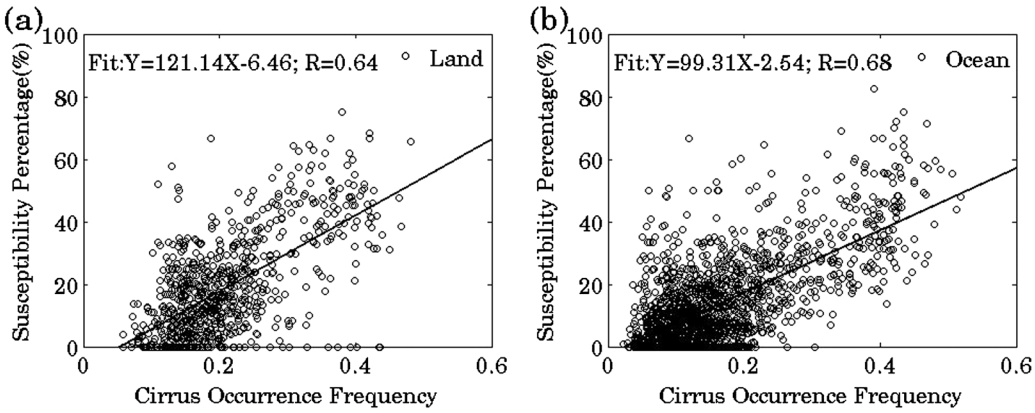

Figure 3. Scatterplot between the Aqua MODIS AOT's susceptibility percentage to cirrus contamination and the CALIPSO-derived thin cirrus occurrence frequency: (a) land and (b) ocean.

Finally, MODIS AOT data are classified into "cirrus-free" and "cirrus-contaminated" groups according to the corresponding CALIPSO cirrus flag. Because cirrus contamination causes AOTs to be overestimated and leads to larger sized particles in the size distribution, we investigated the corresponding changes in AOT and Ångström exponent (AE), in addition to susceptibility percentage (SP, an indicator of the percentage of best quality assured aerosol retrievals that are potentially contaminated by cirrus) in response to thin cirrus contamination. Due to large data uncertainties in the land AE products, we only examined AE over ocean. Table 1 summarizes the main global average statistics on the susceptibility of MODIS aerosol retrievals to thin cirrus contamination and its sensitivity to seasonality and sampling methods. Figure 2 highlights the global spatial patterns of the SP values for the MODIS Dark Target and Deep Blue aerosol retrievals, respectively.

[16] The spatial patterns of the susceptibility (Figure 2) seem to resemble that of thin cirrus occurrence frequency (Figure 1). Higher susceptibility of aerosol retrievals to thin cirrus is found in the tropics (20°S–20°N), where thin cirrus clouds usually occur more frequently. A statistically significant positive relationship between the CALIPSO-derived thin cirrus occurrence frequency (Figure 1) and the MODIS susceptibility percentage (as seen in Figure 2) was observed and is shown in Figure 3. The positive correlation implies potential thin cirrus contamination in the MODIS aerosol retrievals. The higher the thin cirrus occurrence is, the more MODIS C5 aerosol retrievals are potentially susceptible to thin cirrus.

[17] As summarized in Table 1, when all-season data were considered for MODIS C5 aerosol pixels with zero cloud fraction, the global averaged SP values for Dark Target AOT (DT-AOT) and Deep Blue AOT (DB-AOT) were calculated with two approaches: (1) "sample-weighted" (SW) approach that gives equal weight to each MODIS/CALIPSO coincidence. This means statistics are calculated from all coincidences while sample size can vary from grid to grid, and from land to ocean; (2) "grid-weighted" (GW) approach that gives equal weight to each 5° × 5° grid box. In this approach, all the samples at each grid are averaged first before the statistics are calculated. This means the statistics are computed after the samples have been gridded (5° × 5° boxed region), thus the statistical contribution from each grid is equal. In the "sample-weighted" approach, the SP values are 3.19% (12.70% over land and 1.93% over

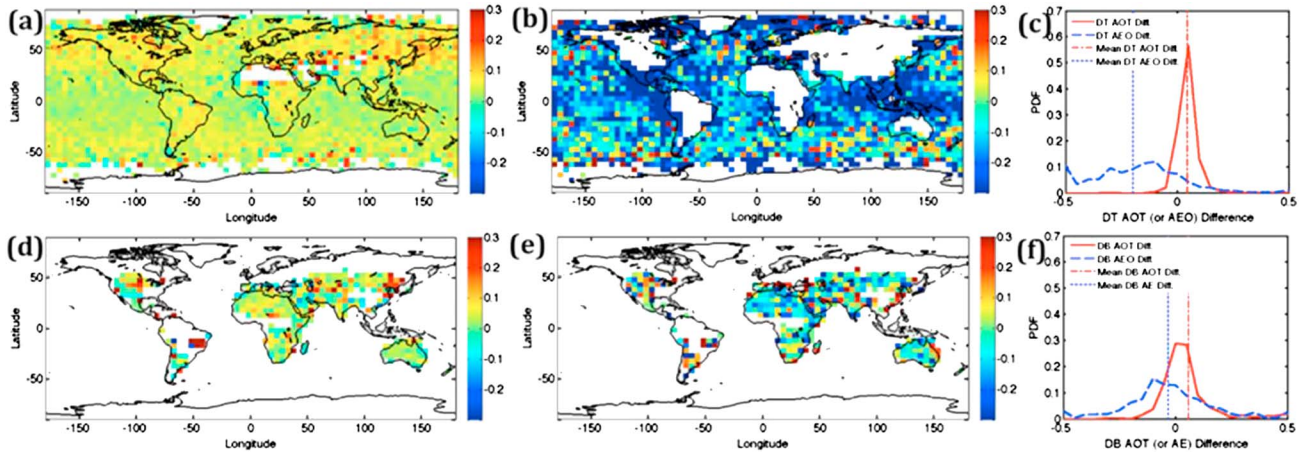

Figure 4. Composites and probability distribution function (PDF) of the differences between cirrus-contaminated cases and cirrus-free cases: (a) DT-AOT, (b) DT-AEO, and (c) PDF of Figures 4a and 4b. (d–f) Similar to Figures 4a–4c except they are for Deep Blue products.

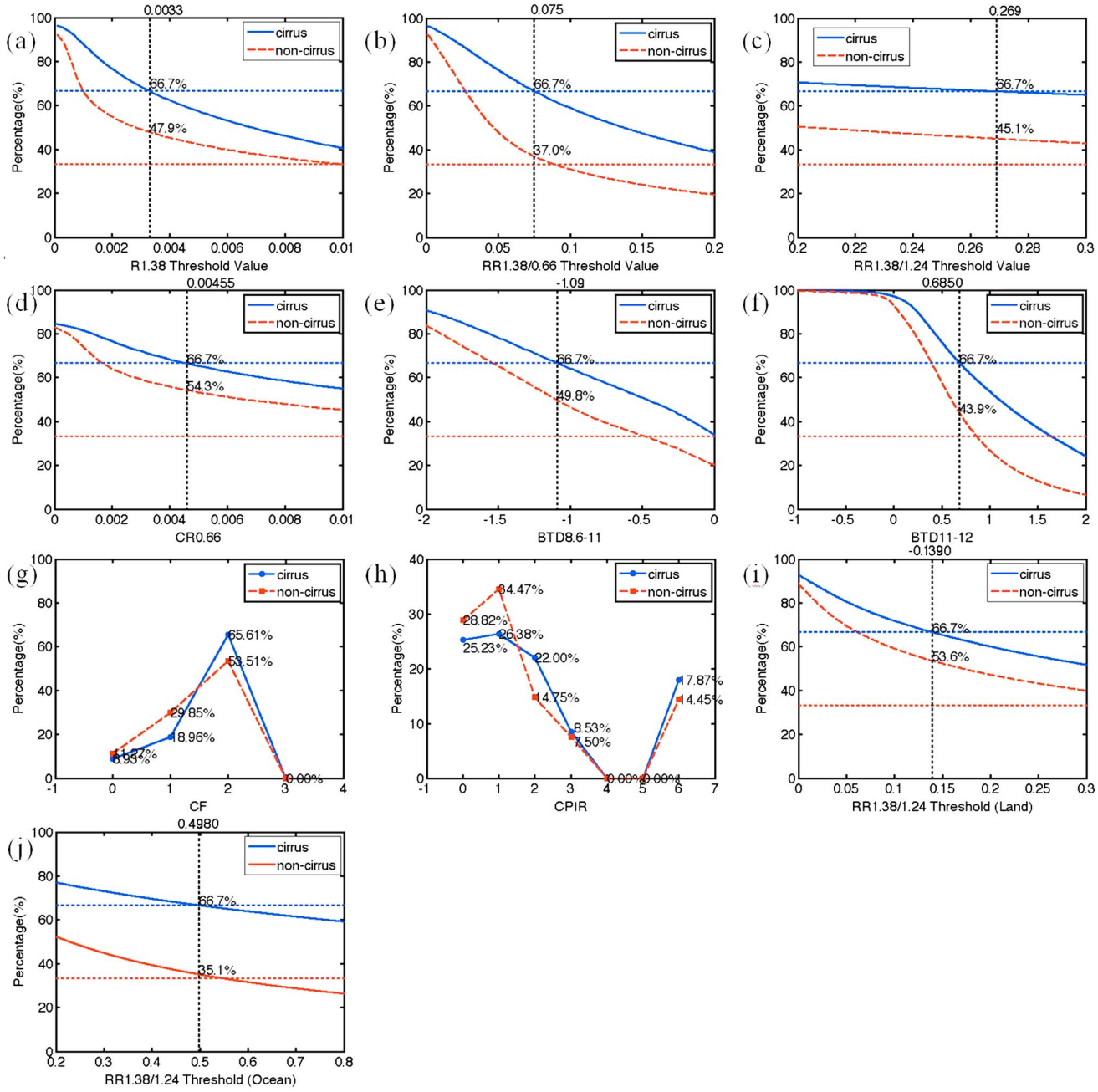

Figure 5. Effectiveness and robustness of eight MODIS-derived cirrus-screening parameters for cirrus screening: (a) R1.38, (b) RR1.38/0.66, (c) RR1.38/1.24, (d) CR0.66, (e) BTD8.6-11, (f) BTD11-12, (g) CF, (h) CPIR, (i) RR1.38/1.24 (land), and (j) RR1.38/1.24 (ocean). Numbers on the vertical lines are threshold values and corresponding cirrus detection % (blue, as close to 67%) and false detection % (red, the less the better).

ocean) for DT-AOT and 5.73% for DB-AOT, respectively. The DT-AOT difference between "cirrus-free" and "cirrus-contaminated" cases is 0.0603 (0.0715 over land and 0.0467 over ocean), higher than the estimate of 0.025 of total cloud contamination assessed in *Kaufman et al.* [2005]. For Deep Blue, however, this difference is about 0.0719, owing to relatively higher aerosol loadings and data uncertainties at or near aerosol sources. Changes in the AE and Fine Mode Fraction (FMF) over ocean between "cirrus-contaminated" and "cirrus-free" cases are also seen with negative signs in Table 1, indicating a greater number of large particles in the retrievals, possibly attributed to cirrus contamination. Similarly, the differences between "cirrus-free" and "cirrus-contaminated" cases in AOT and AE averages are demonstrated in Figure 4. The overall AOT changes are positive (Figures 4a and 4d) while the overall AE changes are negative (Figures 4b and 4e). Positive AOT and negative AE changes are also evident in the probability data distributions shown in Figures 4c and 4f, which indicate cirrus contamination. It is noteworthy that the results with MYD04 zero cloud fractions are conservative evaluations and potential thin cirrus contamination could also occur for those quality-filtered aerosol retrievals in partially cloudy pixels. However, the difference in spatial resolution of MODIS (10 km for aerosol products)

Table 2. Robustness of Eight MODIS-Derived Parameters in Their Thin Cirrus Screening Performance Evaluated Against CALIPSO Cirrus Identification[a]

	R1.38	**RR1.38/0.66**	RR1.38/1.24	RR1.38/1.24 (land)	**RR1.38/1.24 (ocean)**	BTD 8.6–11	**BTD 11–12**	CR 0.66	CF	CPIR
Threshold value	0.0033	**0.075**	0.269	0.139	**0.498**	−1.09	**0.685**	0.00455	2	2,4
Thin cirrus detection rate	66.7%	**66.7%**	66.7%	66.7%	**66.7%**	66.7%	**66.7%**	66.7%	65.6%	22.0%
Thin cirrus false detection rate	47.9%	**37.0%**	45.1%	53.6%	**35.1%**	49.8%	**43.9%**	54.3%	53.5%	14.8%

[a]The preferable MODIS-derived thin cirrus screening parameters are highlighted in bold.

and CALIPSO (70 m ground footprint diameter) complicates similar evaluations for those cloudy pixels. It is also noteworthy that the number of collocated samples varies geographically and may impact the statistical significance of the results. For example, sunglint results in very few collocated samples over oceans during summer in the northern midlatitudes [*Kittaka et al.*, 2011; *Redemann et al.*, 2012]. Because the susceptibility percentage in Figure 2 is a ratio-based parameter and we used more than 5 years of CALIPSO data for matching up, the sample size impact did not produce any significant spatial features in Figure 2. Similarly, no significant spatial patterns related to sunglint migration were observed as shown in Figure 2.

3.2. Evaluation of Eight MODIS-Retrieved Cirrus Screening Parameters

[18] Detecting cirrus using the eight MODIS-retrieved cirrus screening parameters (R1.38, RR1.38/0.66, RR1.38/1.24, BTD8.6–11, BTD11–12, CR0.66, CF, and CPIR) was tested against the CALIPSO cirrus identification cases to examine their cirrus detection and false detection rates. Statistical results from the 1 year of data are shown in Figure 5 and Table 3.

[19] For the flag-based methods (i.e., CF and CPIR), the cirrus detection rate can be calculated directly by taking a ratio of the number of consistent cirrus cases from both CF (or CPIR) and CALIPSO to the total number of cirrus cases from CALIPSO. In contrast, the false detection rate is calculated by taking a ratio of the number of non-thin-cirrus cases from CALIPSO that are misidentified by CF (or CPIR) as cirrus cases over the total number of non-thin-cirrus cases from CALIPSO. For the remaining six parameters, however, threshold values have to be defined before they are implemented for cirrus screening. Examining the robustness of these parameters is achieved by comparing their false detection rates at the same threshold values, for example, setting their cirrus detection rates to two thirds (66.7%). The parameter with the lowest false detection rate can minimize the cirrus false detection while at the same time maintaining a comparable level of successful cirrus screening. The threshold values for the cirrus screening parameters are listed in Table 2. For the six threshold value-based tests, the pixels that have a higher value of the cirrus screening parameter than the corresponding threshold value are flagged as thin cirrus and screened out before the aerosol retrieval (see equation (1)). For the two flag-based tests, pixels

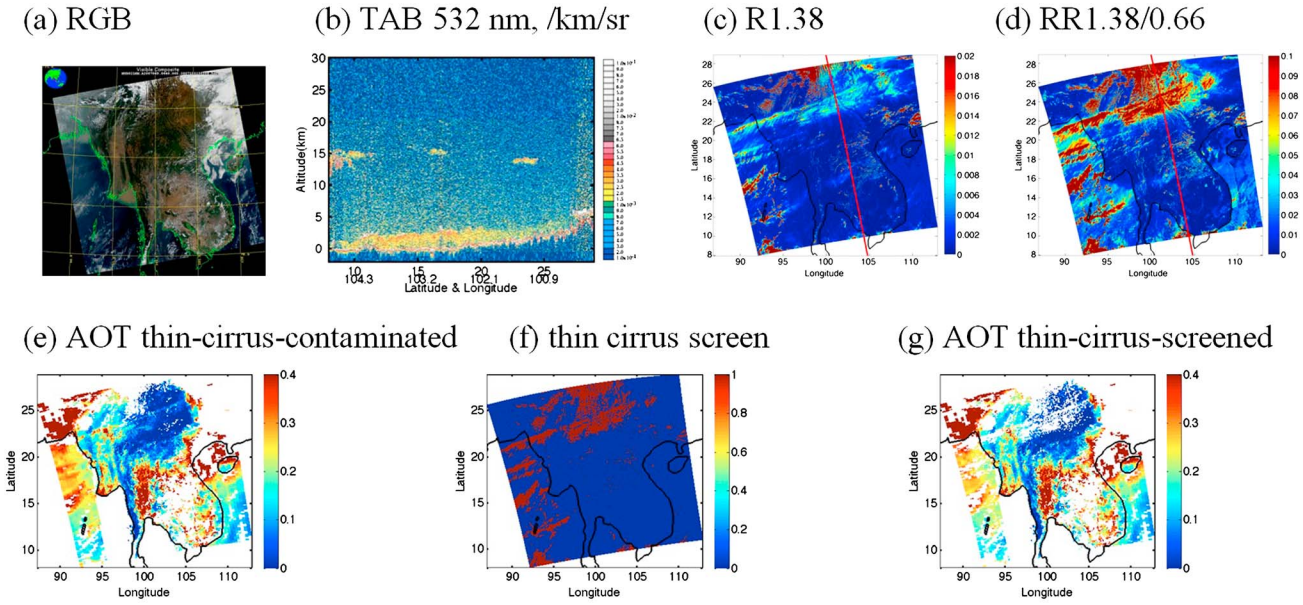

Figure 6. A thin cirrus underscreening case and corresponding improved screening in the MODIS AOT measurements: (a) RGB, (b) total attenuated backscatter (TAB) at 532 nm, (c) R1.38, (d) RR1.38/0.66, (e) "thin cirrus contaminated" AOT retrievals, (f) the new thin cirrus flag using RR1.38/0.66, and (g) "thin cirrus screened" AOT retrievals with the new thin cirrus flag of Figure 6f. The case was over Southeast Asia on 18 February 2007. The red lines that cross the granules in Figures 6c and 6d are the CALIPSO overpass tracks.

having the same exact parameter flag values are identified as thin cirrus and thus are screened out before the aerosol retrieval is performed (see equations (2) and (3)).

[20] For six threshold value-based parameters:

$$\text{Thin Cirrus} : P >= P_{threshold}; \text{Non-Thin-Cirrus} : P < P_{threshold}. \quad (1)$$

$$\text{For Cirrus Flag (CF)} : \text{Thin Cirrus} : CF = 2; \text{Non-Thin-Cirrus}, CF \neq 2. \quad (2)$$

$$\text{For Cloud Phase Infrared (CPIR)} : \text{Thin Cirrus} : CPIR = 2 \text{ or } 4; \text{Non-Thin-Cirrus}, CPIR \neq 2 \text{ or } 4. \quad (3)$$

[21] In Figure 5, the performance of each cirrus screening parameter is demonstrated as functions of threshold values for threshold-based parameters or flags (i.e., CF and CPIR flags). The horizontal blue (or red) dashed lines correspond to two third (or one third) of cirrus detection rates. The blue and red curves are equations of cirrus detection rates (positive or false detection rates) as functions of threshold values (or flags to CF and CPIR). A reasonable cirrus screening parameter with an appropriate threshold value should achieve at least a two thirds cirrus detection rate with the lowest false detection rate possible. As seen in Figure 5 and Table 2, the CF test yields a reasonably high cirrus detection success rate (65.6%), but its false detection rate is also high (53.5%), which means it will cause significant overscreening if it is employed for operational cirrus screening. The CPIR test does have a low false detection rate, but it only identifies 22.0% of cirrus cases, which means it will significantly underscreen cirrus if it is employed for operational cirrus screening. Among the remaining six parameters, the test based on RR1.38/0.66 achieves the best overall performance with the lowest false detection rate of 37.0% at a threshold value of 0.075. It is followed by BTD11–12 (43.9%), RR1.38/1.24 (45.1%), R1.38 (47.9%), BTD8.6–11 (49.8%), and CR0.66 (54.3%).

[22] In the study, we also found that RR1.38/1.24 should have different threshold values over land and ocean, respectively, because R1.24 is much lower over ocean than over land, while R1.38 is not as sensitive to surface features as R1.24. In other words, RR1.38/1.24 has much higher values over ocean than over land, and therefore it should be treated separately for evaluating cirrus screening performance. Also, from Figure 5 and Table 2, RR1.38/1.24 seems to perform better over ocean than over land, with 35.1% versus 53.6% in the false detection rates, respectively, while maintaining the same cirrus detection rates of 66.7%.

[23] Requiring only a single threshold value for both land and ocean, RR1.38/0.66 is preferred overall. A threshold value of 0.075 is recommended for RR1.38/0.66 to maintain a two thirds success rate in identifying cirrus. If we do not consider different threshold values over land and ocean separately, the second preference goes to BTD11–12. This parameter is expected to be useful when R1.38 "sees" surface or dense aerosol features other than cirrus clouds if atmospheric columnar water vapor is too low to attenuate the signals at this wavelength. BTD11–12, with a threshold value of 0.685, can achieve a two thirds success rate in identifying cirrus while maintaining a relatively low false detection rate. As an additional test, we calculated thin cirrus occurrence frequency using the recommended RR1.38/0.66 test with a threshold of 0.075. The resultant map (figure not shown) shows similar cirrus occurrence frequency as in Figure 1, in both magnitude and regional variations.

3.3. Examples of Cirrus Screening Using RR1.38/0.66

[24] To demonstrate the implementation of the recommended cirrus screening using RR1.38/0.66 which is the most preferred performance as discussed earlier, an example is presented in Figure 6. The observation was on 18 February 2007 over Southeast Asia where atmospheric water vapor is sufficiently high to attenuate R1.38 due to the strong water vapor absorption at this middle infrared band. Hence, R1.38 can be used to effectively discriminate cirrus and noncirrus scenes.

[25] Cirrus contamination in the MODIS AOT measurements and corresponding screening and corrections are observed in the example over Southeast Asia (Figure 6). High thin cirrus clouds usually have an optical thickness less than 0.3 and can reach altitudes higher than 10 km in the tropics. Because they are bluish colored and sometimes subvisual, it is difficult to observe these clouds in an RGB image (Figure 6a). However, the thin cirrus features are clearly identifiable in the collocated CALIPSO measurement. As shown in Figure 6b, the CALIPSO 532 nm total attenuated backscatter detected high thin cirrus around 101°E, 24°N, where aerosol signals were relatively low, further evidenced in the CALIPSO VFM products. On the other hand, both R1.38 and RR1.38/0.66 also clearly show the existence of thin cirrus clouds. Particularly noted is the large cirrus coverage across the northern part of the granule over land (between 20°N and 25°N) and the smaller coverage at the western edge of the granule over ocean (between 15°N and 20°N) (Figures 6c and 4d). The cirrus coverage becomes more prominent using the RR1.38/0.66 measurement (Figure 4d), a favorable cirrus detection variable [e.g., *Roskovensky and Liou*, 2003; *Huang et al*., 2011]. The current cloud screening of the MODIS aerosol could not screen out these cirrus clouds effectively, as demonstrated in Figure 6e. A thin cirrus flag was developed using RR1.38/0.66 with a threshold value of 0.075 (Figure 6f). An image of AOT with the updated cirrus screening scheme using the RR1.38/0.66 test is presented in Figure 6g, which shows that the RR1.38/0.66 test successfully screened out those thin cirrus clouds identified by CALIPSO without introducing significant cirrus overscreening.

4. Summary and Discussions

[26] Susceptibility of the Aqua-MODIS operational aerosol products to thin cirrus contamination was evaluated using concurrent cirrus observations from CALIPSO within the A-Train constellation. Similar to the finding from the assessment by *Kaufman et al*. [2005], the comparison with the CALIPSO cirrus identification in this paper indicated that Aqua MODIS Collection 5 aerosol retrievals are also subject to residual thin cirrus contamination. The susceptibility percentages for Dark Target and Deep Blue retrievals are about 3.2% and 5.7%, respectively, in global averages, while they show a strong regional dependence and vary between land and ocean. The MODIS aerosol measurements are more susceptible to cirrus contamination in the cirrus-cloud prevailing regions, particularly in the tropical regions (20°S–20°N), such as Southeast Asia, Central Africa, Central America, and Western Pacific, and it occurs more profoundly in thin cirrus active seasons. Such linkage between the susceptibility of MODIS aerosol retrievals to the CALIPSO-derived thin cirrus

occurrence frequency implies potential thin cirrus contamination in the MODIS aerosol retrievals. The AOT differences between "cirrus-free" and "cirrus-contaminated" cases are about 0.060 and 0.072, respectively, in the global averages for the Dark Target product and the Deep Blue product.

[27] By testing against the cirrus identifications from CALIPSO, we further evaluated the effectiveness and robustness of eight MODIS-derived parameters in thin cirrus screening. For a universal threshold value selection over both land and ocean, RR1.38/0.66 is preferred overall, followed by BTD11–12, while RR1.38/1.24 achieves competitive performance over ocean. With a recommended threshold value of 0.075, RR1.38/0.66 can achieve a two thirds success rate in identifying cirrus while minimizing cirrus false detection. A combination of RR1.38/0.66 and BTD11–12 is recommended as an alternative for the thin cirrus screening when the columnar water vapor in the atmosphere is low, and R1.38 "sees" surface or aerosol features other than thin cirrus.

[28] The case studies presented demonstrated that the MODIS Collection 5 aerosol retrieval can be improved with these proposed thin cirrus screening schemes. More systematic and thorough evaluations are recommended to quantify the possible improvement in the aerosol retrieval with the proposed thin cirrus screening schemes for the upcoming MODIS Collection 6 aerosol retrievals.

[29] **Acknowledgments.** This work is supported by grant from the NASA EOS Program, managed by Hal Maring. Authors thank Brent N. Holben, Alexander Smirnov, Ellsworth J. Welton, Robert C. Levy, David M. Giles, Bo-Cai Gao, Steve Ou, James R. Campbell, and Zhien Wang for their constructive comments on the use of in situ and satellite data, analysis methodology, and cirrus climatology. The authors thank three anonymous reviewers for their constructive and insightful comments that lead to the significant improvements of the paper. Aqua MODIS L1B and L2 data were obtained from NASA L1 and Atmosphere Archive and Distribution System (LAADS). CALIPSO data were obtained from the NASA Langley Research Center Atmospheric Science Data Center.

References

Andreae, M. O. (1991), Biomass burning: Its history, use, and distribution and its impact on environmental quality and global change, in *Global Biomass Burning: Atmospheric, Climatic, and Biospheric Implications*, edited by J. S. Levine, pp. 3–21, MIT Press, Cambridge, Mass.

Breon, F.-M., D. Tanre, and S. Generso (2002), Aerosol effect on cloud droplet size monitored from satellite, *Science*, *295*, 834–838.

Chew, B. N., J. R. Campbell, J. S. Reid, D. M. Giles, E. J. Welton, S. V. Salinas, and S. C. Liew (2011), Tropical cirrus cloud contamination in sun photometer data, *Atmos. Environ.*, *45*, 6724–6731.

Gao, B. C., and Y. Kaufman (1995), Selection of the 1.375 μm MODIS channel for remote sensing of cirrus clouds and stratospheric aerosols from space, *J. Atmos. Sci.*, *52*, 4231–4237.

Gao, B. C., Y. Kaufman, D. Tanre, and R.-R. Li (2002a), Distinguishing tropospheric aerosols from thin cirrus clouds for improved aerosol retrievals using the ratio of 1.38μm and 1.24-μm channels, *Geophys. Res. Lett.*, *29*(18), 1890, doi:10.1029/2002GL015475.

Gao, B. C., P. Yang, W. Han, R.-R. Li, and W. J. Wiscombe (2002b), An algorithm using visible and 1.38-μm channels to retrieve cirrus cloud reflectances from aircraft and satellite data, *IEEE Trans. Geosci. Remote Sens.*, *40*(18), 1659–1668.

Hsu, N.C., S.-C. Tsay, M. D. King, and J. R. Herman (2004), Aerosol properties over bright-reflecting source regions, *IEEE Trans. Geosci. Remote Sens*, *42*(3), 557–569.

Hsu, N. C., S.-C. Tsay, M. D. King, and J. R. Herman (2006), Deep Blue retrieval of Asian aerosol properties during ACE-Asia, *IEEE Trans. Geosci. Remote Sens.*, *44*(11), 3180–3195.

Huang, J., N. C. Hsu, S. Tsay, M. Jeong, B. N. Holben, T. A. Berkoff, and E. J. Welton (2011), Susceptibility of aerosol optical thickness retrievals to thin cirrus contamination during the BASE-ASIA campaign, *J. Geophys. Res.*, *116*, D08214, doi:10.1029/2010JD014910.

Huang, J., et al. (2012), Evaluations of cirrus contamination and screening in ground aerosol observations using collocated lidar systems, *J. Geophys. Res.*, *117*, D15204, doi:10.1029/2012JD017757.

Jeong, M. J., and Z. Li (2005), Quality, compatibility and synergy analyses of global aerosol products derived from the advanced very high resolution radiometer and total ozone mapping spectrometer, *J. Geophys. Res.*, *110*, D10S08, doi:10.1029/2004JD004647.

Jeong, M. J., Z. Li, D. A. Chu, and S.-C. Tsay (2005), Quality and compatibility analyses of global aerosol products derived from the advanced very high resolution radiometer and moderate resolution imaging spectroradiometer, *J. Geophys. Res.*, *110*, D10S09, doi:10.1029/2004JD004648.

Jiang, J. H., et al. (2010), Five-year (2004–2009) observations of upper tropospheric water vapor and cloud ice from MLS and comparisons with GEOS-5 analyses, *J. Geophys. Res.*, *115*, D15103, doi:10.1029/2009JD013256.

Kaufman, Y. J., et al. (2005), A critical examination of the residual cloud contamination and diurnal sampling effects on MODIS estimates of aerosol over ocean, *IEEE Trans. Geosci. Remote Sens.*, *43*(12), 2886–2897.

Kittaka, C., D. M. Winker, M. A. Vaughan, A. Omar, and L. A. Remer (2011), Intercomparison of column aerosol optical depths from CALIPSO and MODIS-Aqua, *Atmos. Meas. Tech.*, *4*, 131–141, doi:10.5194/amt-4-131-2011.

L'Ecuyer, T. S., and J. H. Jiang (2010), Touring the atmosphere aboard the A-Train, *Phys. Today*, *63*(7), 36–41.

Levy, R. C., L. A. Remer, R. G. Kleidman, S. Mattoo, C. Ichoku, R. Kahn, and T. F. Eck (2010), Global evaluation of the Collection 5 MODIS dark-target aerosol products over land, *Atmos. Chem. Phys.*, *10*(21), 10,399–10,420.

Liu, Z., A. Omar, Y. Hu, M. A. Vaughan, and D. M. Winker (2005), CALIOP Algorithm Theoretical Basis Document, part 3: Scene classification algorithms, technical report, NASA Langley Res. Cent., Hampton, Va., [Available at http://www-calipso.larc.nasa.gov/resources].

Liu, Z., et al. (2009), The CALIPSO lidar cloud and aerosol discrimination: Version 2 algorithm and initial assessment of performance, *J. Atmos. Oceanic Technol.*, *26*, 1198–1213.

Massie, S. T., J. Gille, C. Craig, R. Khosravi, J. Barnett, W. Read, and D. Winker (2010), HIRDLS and CALIPSO observations of tropical cirrus, *J. Geophys. Res.*, *115*, D00H11, doi:10.1029/2009JD012100.

Menon, S., J. Hansen, L. Nazarenko, and Y. Luo (2002), Climate effects of black carbon aerosols in China and India, *Science*, *297*, 2250–2253.

Menzel, W. P., R. A. Frey, and B. A. Baum (2013), Cloud top properties and cloud phase: Algorithm theoretical basis document, NASA Goddard Space Flight Cent., Greenbelt, Md., [Available at http://modis-atmos.gsfc.nasa.gov/reference_atbd.html].

Myhre, G., et al. (2005), Intercomparison of satellite retrieved aerosol optical depth over ocean during the period September 1997 to December 2000, *Atmos. Chem. Phys.*, *5*, 1697–1719.

Redemann, J., M. A. Vaughan, Q. Zhang, Y. Shinozuka, P. B. Russell, J. M. Livingston, M. Kacenelenbogen, and L. A. Remer (2012), The comparison of MODIS-Aqua (C5) and CALIOP (V2 & V3) aerosol optical depth, *Atmos. Chem. Phys.*, *12*, 3025–3043, doi:10.5194/acp-12-3025-2012.

Remer, L. A., et al. (2005), The MODIS aerosol algorithm, products and validation, *J. Atmos. Sci. Spec. Sect.*, *62*, 947–973.

Remer, L. A., D. Tanre, Y. J. Kaufman, R. Levy, and S. Mattoo (2009), Algorithm for remote sensing of tropospheric aerosol from MODIS for collection 005: revision 2 products: 04_L2, ATML2, 08_D3, 08_E3, 08_M3, NASA Goddard Space Flight Cent., Greenbelt, Md, [Available at http://modis-atmos.gsfc.nasa.gov/reference_atbd.html].

Roskovensky, J. K., and K. N. Liou (2003), Detection of thin cirrus from 1.38 mm/0.65 mm reflectance ratio combined with 8.6–11 mm brightness temperature difference, *Geophys. Res. Lett.*, *30*(19), 1985, doi:10.1029/ 2003GL018135.

Roskovensky, J. K., K. N. Liou, T. J. Garrett, and D. Baumgardner (2004), Simultaneous retrieval of aerosol and thin cirrus optical depths using MODIS airborne simulator data during CRYTAL-FACE and CLAMS, *Geophys. Res. Lett.*, *31*, L18110, doi:10.1029/2004GL020457.

Sassen, K., and J. R. Campbell (2001), A midlatitude cirrus cloud climatology from the facility for atmospheric remote sensing. Part I: Macrophysical and synoptic properties, *J. Atmos. Sci.*, *58*, 481–496.

Sassen, K., Z. Wang, and D. Liu (2008), Global distribution of cirrus clouds from CloudSat/Cloud-Aerosol Lidar and Infrared Pathfinder Satellite Observations (CALIPSO) measurements, *J. Geophys. Res.*, *113*, D00A12, doi:10.1029/2008JD009972.

Schaap, M., A. Apituley, R. M. A. Timmermans, R. B. A. Koelemeijer, and G. de Leeuw (2009), Exploring the relation between aerosol optical depth and PM2.5 at Cabauw, the Netherlands, *Atmos. Chem. Phys.*, *9*, 909–925, doi:10.5194/acp-9-909-2009.

Takemura, T., T. Nozawa, S. Emori, T. Y. Nakajima, and T. Nakajima (2005), Simulation of climate response to aerosol direct and indirect effects with aerosol transport-radiation model, *J. Geophys. Res.*, *110*, D02202, doi:10.1029/2004JD005029.

Tao, W.-K., X. Li, A. Khain, T. Matsui, S. Lang, and J. Simpson (2007), Role of atmospheric aerosol concentration on deep convective precipitation: Cloud-resolving model simulations, *J. Geophys. Res.*, *112*, D24S18, doi:10.1029/2007JD008728.

Vaughan, M. A., et al. (2005), CALIOP algorithm theoretical basis document, part 2: Feature detection and layer properties algorithms, *Rep. PC-SCI-*

202.02, 87 pp., NASA Langley Res. Cent., Hampton, Va. [Available at http://www-calipso.larc.nasa.gov/resources/project_documentation.php].

Vaughan, M. A., et al. (2009), Fully automated detection of cloud and aerosol layers in the CALIPSO lidar measurements. *J. Atmos. Oceanic Technol.*, *26*, 2034–2050.

Winker, D. M., et al. (2010), The CALIPSO mission: A global 3D view of aerosols and clouds, *Bull. Am. Meteorol. Soc.*, *91*, 1211–1229, doi:10.1175/2010BAMS3009.1.

Yorks, J. E., D. L. Hlavka, M. A. Vaughan, M. J. McGill, W. D. Hart, S. Rodier, and R. Kuehn (2011), Airborne validation of cirrus cloud properties derived from CALIPSO lidar measurements: 1. Spatial properties, *J. Geophys. Res.*, *116*, D19207, doi:10.1029/2011JD015942.

Young, S. A., and M. A. Vaughan (2009), The retrieval of profiles of particulate extinction from Cloud Aerosol Lidar Infrared Pathfinder Satellite Observations (CALIPSO) data: Algorithm description, *J. Atmos. Oceanic Technol.*, *26*, 1105–1119, doi:10.1175/2008 JTECHA1221.1.